FT-IR Spectroscopic Detection of Biochemical and Structural Changes Associated with Early Tumor Transformation in Hamster Oral Carcinogenesis

R. Sethupathi[1], M. Gohulkumar[2] and N. Krishnakumar[3,*]

[1]Department of Physics, Vinayaka Mission's Kirupanantha Variar Engineering College, Vinayaka Mission's Research Foundation (Deemed to be University), Salem-636308, India
[2]Department of Physics, Vivekanandha College of Arts and Science for Women (Autonomous), Tiruchengode-637205, India
[3]Department of Physics, Annamalai University, Annamalai Nagar-608002, India

*Corresponding author: E-mail: nskumarphyamu@gmail.com

FT-IR spectroscopy is a vibrational spectroscopic technique that can be used to investigate the biochemical changes at the molecular level in various tissue transformation conditions [hyperplasia, dysplasia and well differentiated squamous cell carcinoma (WDSCC)] with respect to control tissues in DMBA-induced hamster oral carcinogenesis. The results revealed that a significant increase in the amount of proteins and nucleic acid contents and a decrease in the amount of lipids contents are observed in WDSCC when compared to control, hyperplasia, dysplasias. In addition, the detailed secondary structure of proteins in the control and various tissue transformation conditions is also presented. Further, the diagnostic algorithms based on PC-LDA achieved an overall sensitivity of 80-100 % and specificity of 81-100 %. The present study further shows a great potential of FT-IR spectroscopy as a complimentary tool, which may provide a rapid screening method and have potential use in the diagnosis of dysplasia and early, non-invasive oral cancer.

Keywords: Oral carcinogenesis, FT-IR spectroscopy, Principal component-linear discriminant analysis.

INTRODUCTION

Oral cancer is the major cause of mortality and morbidity in developing as well as developed countries with an annual estimated incidence of 275,000 cases, two-thirds of which are from developing countries. Oral squamous cell carcinoma (OSCC) accounts for 90 % of all oral cancers and the risk of developing oral cancer has been shown to increase with age [1]. There is considerable geographical heterogeneity in incidence rates that can be attributed to the differences in the distribution of associated risk factors Betel quid chewing with tobacco, a common practice in India, has been identified as the single most important factor in the aetiology of oral cancer. Recent progress in diagnostic techniques and medical treatments for oral cancer has improved the 5 year survival rate after treatment. The 5-year survival in advance stage cancer after treatment is less than 40 and 80 % in early stage disease. This indicates that detection of oral cancer at an early stage is essential for better outcome of the cancer therapy. Therefore,

it would be of imperative clinical value to develop a real-time, non-invasive, biomolecular and sensitive optical diagnostic technique for improving the early detection of oral precancer and cancer during clinical oral inspections. In this context, a non-invasive optical diagnostic technique providing a direct assessment of biochemical information from suspicious lesion would represent a significant advance in the early detection of oral cancer. These methods are widely used as a tool for analysis of many biological tissues and the technique has been referred to as an "optical biopsy" or "spectral cytopathology" because of its capacity to show features of underlying pathological tissues when compared with normal tissues.

Recently, Fourier transform infrared (FTIR) spectroscopy has emerged as a novel technique that provides information about biochemical changes within cells and tissues *via* characteristic spectral signature changes and can be applied without the use of additional reagents. An FT-IR spectrometer is the instrument used to detect IR light absorbed by molecules. The mid-IR (4000-400 cm^{-1}) is the most commonly used region

for analysis as all molecules possess characteristic absorbance frequencies and molecular vibrations in this range. It measures the absorption of vibrating molecules that have resulted from energy transitions of vibrating dipoles. This technique, being reagent-free, can rapidly and non-invasively detect changes in the biochemical composition of tissues and cells at the molecular level, particularly during carcinogenesis. The resulting spectra are composed of characteristic absorption bands originating from all infrared-active vibrational modes of biomolecules present in the tissues such as proteins, lipids, carbohydrates, glycogen and nucleic acids. In the process of carcinogenesis, these biomolecules show significant variation in their molecular structure and content and these changes should be reflected in the spectra [2]. Further, this technique is especially useful for the analysis of secondary structure of proteins and lipid fluidity in cells and tissues [3-5]. The other advantage of this technique is that it can detect even small alterations in the molecular parameters associated either with the administration of anticancer drugs or with the development of pathologies, which are not easily detected by morphological methods [4-7]. In the past decade, this technique has been successfully applied to the identification of malignancies as well as to discriminate between cancerous and normal tissues for diagnostic purposes in ovary, skin, brain, breast, lung and oral cancers [8-13]. However, the significant FT-IR spectral differences between normal and cancerous tissues are often limited in number and can be difficult to identify and obvious spectral overlapping among all the common spectra. Therefore, powerful and robust spectral data processing and diagnostic algorithms are required to extract significant FT-IR spectral features. In recent years, attempts to quantitative analysis of the FT-IR data using principal component followed by linear discriminant analysis (PC-LDA) can be used. Hence, the present study is designed to investigate the changes in the biochemical and structural changes at the molecular level during various oral tissue transformation conditions (hyperplasia, dysplasia and WDSCC) with respect to control tissues in a hamster oral carcinogenesis model using FT-IR spectroscopy. Further, multivariate analysis, by performing principal component analysis (PCA) for reducing data dimension and linear discriminant analysis (LDA) on the scores of principal component (PC) for the discrimination of control, hyperplasia, dysplasia and WDSCC tissue groups.

EXPERIMENTAL

Sections of various hamster buccal mucosa from 24 samples, obtained from a previous experiment [14,15], were submitted to histological and spectroscopic analysis to determine the composition, the morphology and hence the metabolic changes. One section of each cheek pouch was frozen in liquid nitrogen and stored at -80 °C for further fluorescence spectroscopic analysis. A second portion of the pouch was fixed in 10 % neutral buffered formalin for histopathological studies.

Histological preparation and analysis: The specimens were embedded in paraffin. Sections, 4–5 micrometer in thickness, were cut on a rotary microtome and stained with hematoxylin and eosin (H&E) to observe general pathology features and morphology. The histopathology results confirmed

that 6 were diagnosed as control, 6 were diagnosed as hyperplasia, 6 were diagnosed as dysplasia (1 mild dysplasia, 2 moderate dysplasias and 3 severe dysplasias) and 6 were WDSCC (results not shown). For the final evaluation, only specimens in which pathologist agreed on the diagnosis were used. The spectroscopic data was further classified according to the histological diagnosis.

FT-IR spectroscopic analysis: The FT-IR spectra of hamster buccal pouch tissue samples (control, hyperplasia, dysplasia and WDSCC) were recorded from CAS in Marine Biology, Faculty of Marine Sciences, Annamalai University, Parangipettai, Tamil Nadu, India, using SHIMADZU-8400. The spectrometer was continuously purged with dry nitrogen to eliminate atmospheric water vapour and carbon dioxide. A spectrum was taken as an 142 average of 128 scans to increase the signal to noise ratio. Background spectra, which were collected under identical conditions, were subtracted from the sample spectra automatically. The frequencies for all sharp bands were accurate to 0.01 cm^{-1}. Each sample was scanned with three different points under identical conditions and all of which gave identical spectra. These replicates were averaged and used for further analysis. For detailed data analysis, non-normalized spectra were used. To remove the noise, the spectra were first smoothed with a eight point Savitzky-Golay smoothed function. In determination of the mean values for the peak positions and band areas values, the spectra belonging to each individual of the group were considered. The band positions were measured using the frequency corresponding to the center of weight of each band. Band areas were calculated from smoothed and baseline corrected spectra using ORIGIN 8.0 software. After analysis, the spectra were baseline corrected and normalized with respect to specific bands for visual demonstration. All spectral manipulations were performed using the ORIGIN 8.0 software.

Sample preparation: The buccal mucosa was dried in a freeze dryer (LARK, Penguin Classic Plus, India) overnight in order to remove the water content in the samples. The samples were then ground in an agate mortar and pestle in order to obtain tissue powder. The tissue powder (5 mg) was mixed with completely dried and mixed with potassium bromide (100 mg) and then the mixture was subjected to a pressure of 10 tonnes for 5 min in an evacuated die to produce a clear transparent KBr disc of 13 mm diameter and 1 mm thickness for use in FT-IR spectrometer [4,16]. All the spectra were recorded in the region of 4000-400 cm^{-1}.

RESULTS AND DISCUSSION

Fig. 1 shows the average normalized FT-IR absorbance spectra of the control and various oral transformations conditions such as hyperplasia, dysplasia and WDSCC tissues in the region 4000-400 cm^{-1}. Infrared spectral differences between these groups are observed at the various peaks throughout the averaged FT-IR spectra. These distinctive FT-IR spectral features could reflect biochemical changes in quantity or structural changes at the molecular level associated with tumor transformation. The FT-IR absorbance spectral bands along with possible assignments of the control and experimental animals in each group are shown in Table-1.

TABLE-1
VIBRATIONAL ASSIGNMENTS OF THE BAND FREQUENCIES PRESENT IN THE IR ABSORPTION
SPECTRA MEASURED FOR THE CONTROL, HYPERPLASIA, DYSPLASIA AND WDSCC TISSUE GROUPS

| Control	Hyperplasta	Dysplasta	WDSCC	Vibrational assignments
3430	3486	3414	3417	O-H Stretching hydrogen bonded intermolecular OH groups
–	–	3310	3302	Mainly N-H stretching (amide A) of proteins
3060	3058	3066	3058	N-H stretching (amide B) of proteins
2942	2926	2917	2917	CH_2 asymmetric stretch: mainly lipids
2860	2854	2851	2863	CH_2 symmetric stretch: mainly lipids
1749	1743	1743	-	Carbonyl C=O stretch: phospholipids
1643	1643	1654	1652	Amide I (protein C=O stretching)
1544	1536	1536	1534	Amide II (protein N-H bend, C-N stretch)
1455	1453	1453	1462	CH_2 bending; lipids & proteins
1235	1238	1238	1235	PO_2^- asymmetric stretching: mainly nucleic acids
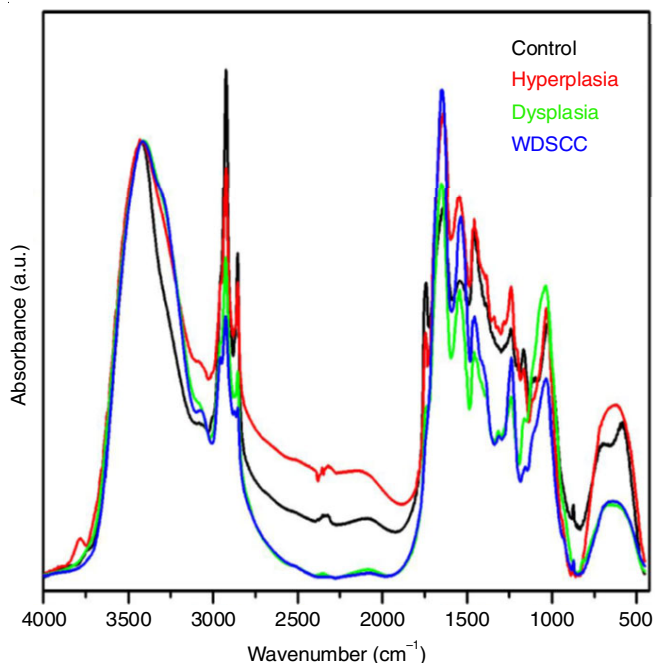
Fig. 1.   Representative FT-IR spectra of the control and the experimental animals in the 4000-400 cm^{-1} region. The spectra were normalized with respect to the band at ~ 3420 cm^{-1}

The prominent infrared absorbance bands observed in control and different pathological tissue groups spectra are characteristic of different vibration modes assumed to represent unique functional groups in cellular molecules including proteins, lipids and nucleic acids. The infrared spectra of buccal mucosa are dominated by many different functional groups of various macromolecules such as lipids, proteins and nucleic acids. To observe the details of the spectral analysis, the FT-

IR spectra were performed in three main spectral ranges corresponding to 3600-3050 cm^{-1} (O-H/N-H stretching region), 3000-2800 cm^{-1} (C-H stretching region) and 1800-800 cm^{-1} (finger print region). This approach allowed us resolve broad, overlapping bands into individual bands thus increasing the accuracy of analysis. The shifts in peak positions and changes in the intensity and more accurately, area values of the bands, give valuable structural and functional information, which may have diagnostic value. The band area and peak position of the selected bands are given in Table-2.

Fig. 2 shows the representative FT-IR spectra of the control and the experimental groups in the 3600-3050 cm^{-1} region. The band observed at 3429 cm^{-1} in the control tissues has been assigned to O-H stretching of proteins and intermolecular H-bonding. This band has been shifted to ~ 3412 cm^{-1} in the WDSCC tissues, which might imply a variation in the hydrogen bonding network in the tumor transformation (Fig. 2). Further, the band centered at ~ 3302 cm^{-1} is assigned to N-H stretching of proteins of amide A [4]. As seen from Fig. 2, this band has been appeared only in dysplasia and WDSCC tissue groups, which may be associated with an increase in the relative amounts of proteins. In addition, the weak band observed at ~ 3070 cm^{-1} represents N-H stretching of proteins of amide B [4].

Fig. 3 shows the average normalized infrared spectra of the control, hyperplasia, dysplasia and WDSCC in the 3000-2800 cm^{-1}, with respect to the band at ~2925 cm^{-1} region. It is well known that this region (3000-2800 cm^{-1}) was used to determine the level of saturation in the lipid acyl chains by examining the changes in C-H stretching band. Two strong peaks at ~ 2925 cm^{-1} and ~ 2855 cm^{-1} were attributed to CH_2 asymmetric and symmetric stretching bands are mainly due to lipids. As can be seen from Fig. 3, these peaks exhibit a lower intensity in the WDSCC tissues when compared to the control

TABLE-2
BAND AREAS VALUES OF THE SELECTED INFRARED BANDS FOR THE CONTROL,
HYPERPLASIA, DYSPLASIA AND WDSCC TISSUE GROUPS

Bend frequency	Control	Hyperplasia	Dysplasia	WDSCC
2934	38.502 ± 3.925	11.855 ± 1.651	9.975 ± 0.629	7.388 ± 0.538
2865	24.657 ± 2.287	3499 ± 0.287	3.641 ± 0.471	2.131 ± 0.271
1660	11.481 ± 1.187	21.607 ± 2.298	14.806 ± 1.387	26.511 ± 2.816
1553	–	17.932 ± 1.738	11.521 ± 1.163	21.468 ± 1.968
1458	26.436 ± 2.198	24.671 ± 2.519	19.675 ± 1.837	14.317 ± 1.837
1238	3.913 ± 0.649	8.345 ± 0.615	13.672 ± 1.296	19.659 ± 2.003

Values are shown as mean ± standard deviation.
The degree of significance was denoted as $p < 0.05$, for comparisons of the control, hyperplasia, dysplasia and WDSCC tissue groups.
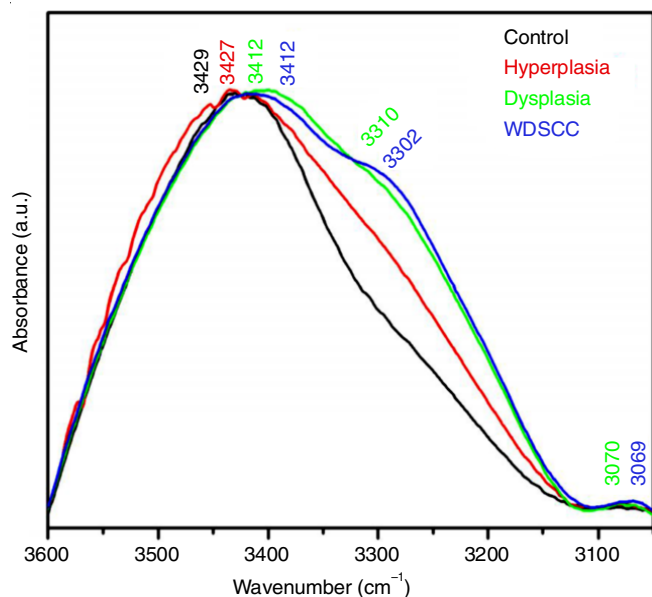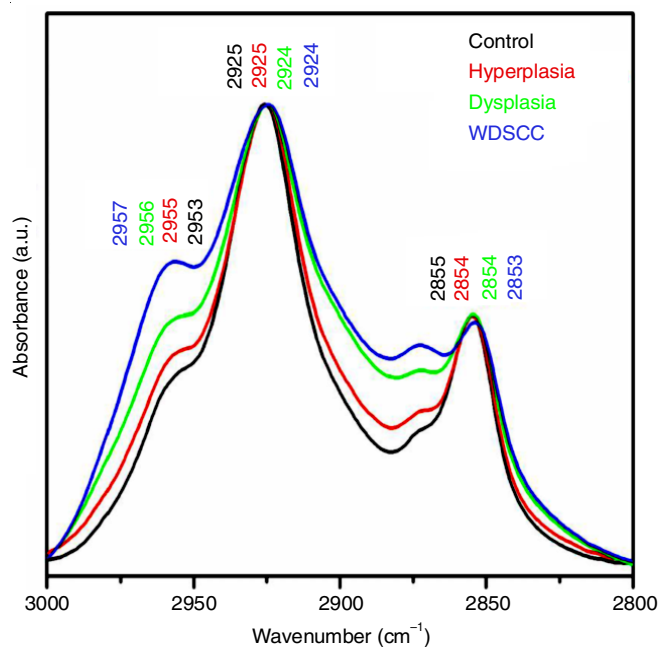
Fig. 2. Representative FT-IR spectra of the control, hyperplasia, dysplasia and WDSCC tissue groups in the 3600-3050 cm^{-1} region. The spectra were normalized with respect to the band at ~ 3425 cm^{-1}

Fig. 3. Representative FT-IR spectra of the control, hyperplasia, dysplasia and WDSCC tissue groups in the 3000-2800 cm^{-1} region. The spectra were normalized with respect to the band at ~ 2925 cm^{-1}

tissues, while the intensity and area of these two bands increase significantly in the hyperplasia and dysplasia tissue groups in comparison to the WDSCC (Fig. 3 and Table-2). This result suggests that tumor progression could be related with a decrease in the relative amounts of lipids.

Investigating infrared absorption spectrum of control, hyperplasia, dysplasia and WDSCC tissues demonstrates the main differences in the finger print (1800-800 cm^{-1}) spectral region are shown in Fig. 4. The finger print region provides a unique spectrum for each group where the position and intensity of the bands are specific for different infrared-active biomolecules. The band centered at ~ 1743 cm^{-1} is assigned to

carbonyl C=O stretching of phospholipids. As seen from Fig. 4, this band has been almost disappeared in WDSCC tumor tissues, which may be associated with a decrease in the relative amounts of phospholipids. In addition, this band has been observed in hyperplasia and dysplasia tissue groups. Further, the major peaks were observed for absorptions in the amide I and amide II regions at ~ 1636 cm^{-1} and ~ 1544 cm^{-1} respectively. The amide I absorption is mainly associated with C=O stretching vibrations [4]. The amide II absorption band arises from amide N-H bending vibration coupled with C-N stretching vibration mode of the polypeptide and protein back bone [4]. A significant increase in the areas of the amide I and amide II bands noticed in the tumor tissues suggest that the tumor tissues may be associated with an increase in the relative amount of proteins. Since the frequency of the amide I band is sensitive to proteins conformation, this band is very useful for the determination of protein secondary structure. The frequency of the amide I band is shifted to higher values in dysplasia and WDSCC tissues (Fig. 4).
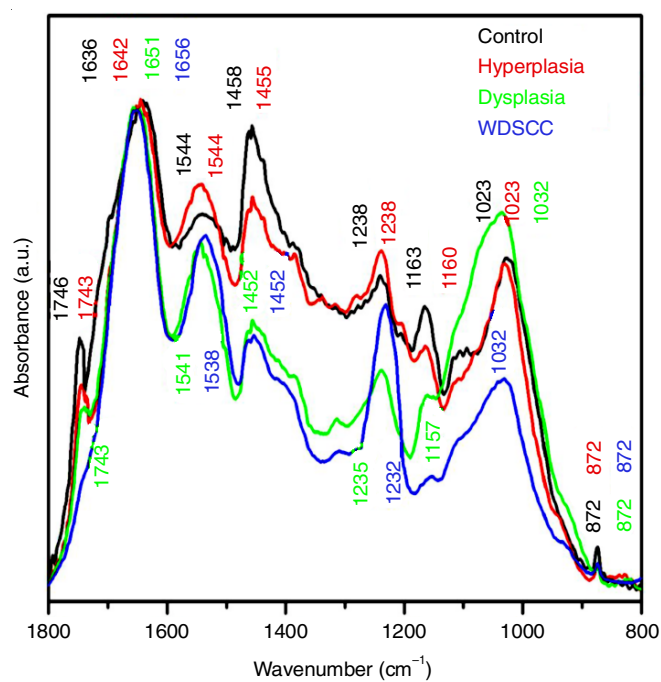

Fig. 4. Representative FT-IR spectra of the control, hyperplasia, dysplasia and WDSCC tissue groups in the 1800-800 cm^{-1} region. The spectra were normalized with respect to the band at ~ 1650 cm^{-1}

To study the secondary structure of proteins in the tissue samples, further analysis has been carried out by resolving the amide I band using the curve fitting method. By taking the second derivative of the arithmetical function, the number of peaks and their relative positions were determined. The average underlying band of amide I band as deduced by curve-fitting analysis for major peaks in the second derivative spectra is given in Fig. 5. The peak located at 1685 cm^{-1} is due to anti-parallel β-sheet structure, the peak located at 1668 cm^{-1} is due to β-turn structure, the peak at 1651 cm^{-1} is assigned to α-helix structure and peak at 1626 cm^{-1} is attributed to aggregate β-sheet structure [4,17]. It is observed (Fig. 6) that the percentage area of β-sheet and β-turn secondary structure increased

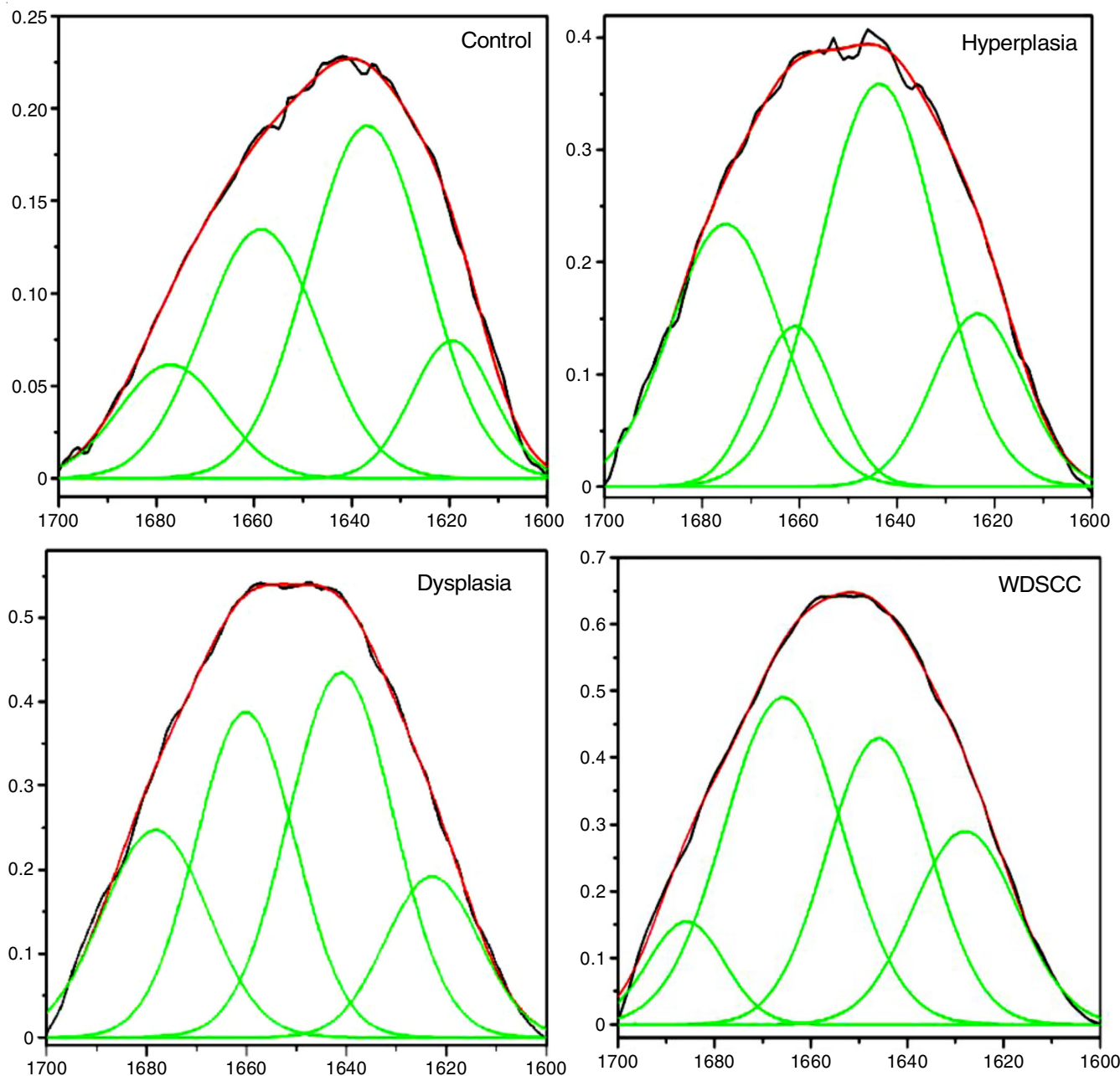Fig. 5. Underlying amide I bands in the 1700 -1600 cm^{-1} region deduced by curve-fitting analysis for average spectra the control, hyperplasia, dysplasia and WDSCC tissue groups

in WDSCC tissues. Further, the percentage area of α-helix structure decreased. These results suggest that WDSCC tissues group causes important changes in the protein profile in favour of β-sheet and β-turn structure. Further, the band observed at ~1232 cm^{-1} in the WDSCC tissues has been assigned to the asymmetric PO$_2^-$ stretching vibrations of the DNA phosphodiester groups [2]. The area of this band increased in DMBA-alone induced tumor tissues when compared to the control tissues (Table-2). Compared to the FT-IR spectra of control and hyperplasia, there were large increases in the content of proteins and nucleic acids in the dysplasia and WDSCC tissue samples.

Further, the multivariate statistical analysis that utilizes the entire spectrum to determine the most diagnostically significant spectral features may improve the diagnostic efficiency of FT-IR spectroscopic technique for tissue analysis. Multivariate statistical techniques based on PC-LDA together with LOOCV were utilized for effective differentiation between the control and the experimental tissues. Canonical discriminant functions that contribute maximally to group separation are identified and substantively interpreted in order to provide meanings for group differentiation. A centroid is a point, which has coordinates that are a group's score on each of the discriminant functions. In the present study, discriminant score plot illustrated in Fig. 7 is a visual display for the classification of IR spectra from the different groups. These tissue spectral differences were explored in greater detail for tissue classification through PC-LDA analysis. Results of the binary classification obtained from PC–LDA are also given in Table-3. Pairwise discriminant function scatter plots for the control and experi-

TABLE-3
CLASSIFICATION EFFICIENCY BETWEEN THE CONTROL, HYPERPLASIA, DYSPLASIA AND WDSCC TISSUE GROUPS

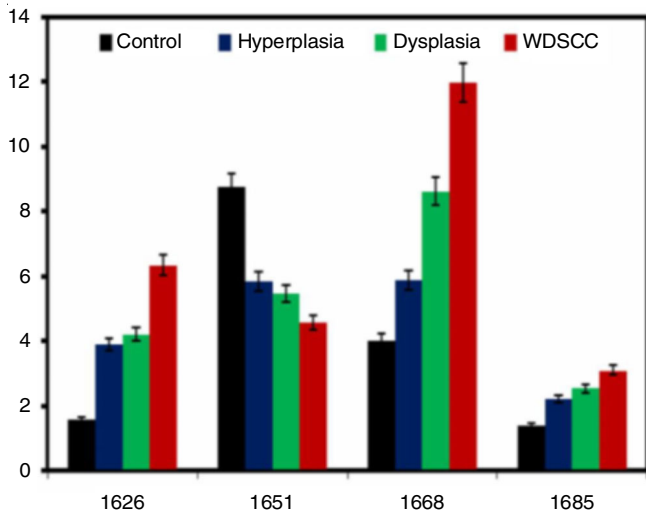| Groups (no. of spectrum = 12)	Control	Hyperplasia	Dysplasisa	WDSCC	Classification efficiency (%)
Control	11	1	0	0	91.6
Hyperplasia	1	10	1	0	83.3
Dysplasia	0	1	10	1	83.3
WDSCC	0	0	3	9	75.0

Fig. 6. Bar diagram of protein secondary stuctural variations for the control, hyperplasia, dysplasia and WDSCC tissue groups. Values are shown as mean ± standard deviation: the degree of significance was denoted as $p < 0.05$, for comparisons of the control, hyperplasia, dysplasia and WDSCC tissue groups
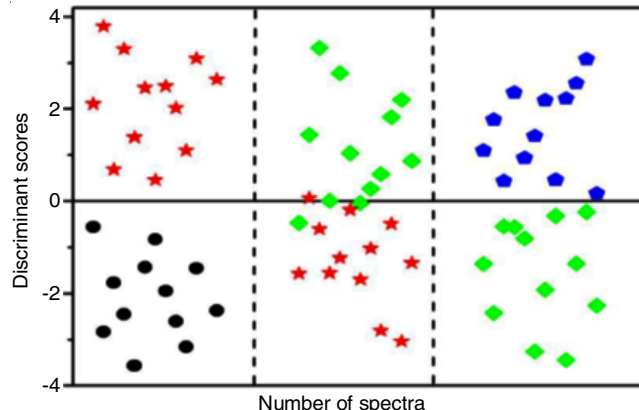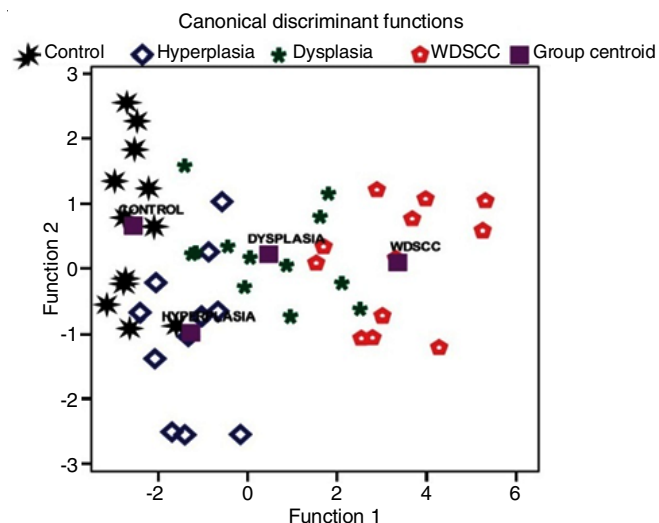

Fig. 7. Canonical discriminant of the function 1 *vs.* function 2 discriminance values for each groups are plotted

Fig. 8. Pair-wise discriminant function scatter plot of different group pairs of control *vs.* hyperplasia, hyperplasia *vs.* dysplasia and dysplasia *vs.* WDSCC tissue groups

TABLE-4
DIAGNOSTIC ACCURACIES OBTAINED FOR THE DISCRIMINATION OF THE CONTROL, HYPERPLASIA, DYSPLASIA AND WDSCC TISSUE GROUPS

Groups	Sensitivity (%)	Specificity (%)	Accuracy (%)
Control *vs.* Hyperplasia	100	100	100
Hyperplasia *vs.* Dysplasia	80.95	81.18	81.39
Dysplasia *vs.* WDSCC	85.71	90.0	87.80

very close to 1 (1.00, 0.92 and 0.96), (Fig. 9) indicating that the approaches are suitable for discriminating between the control and the experimental groups.
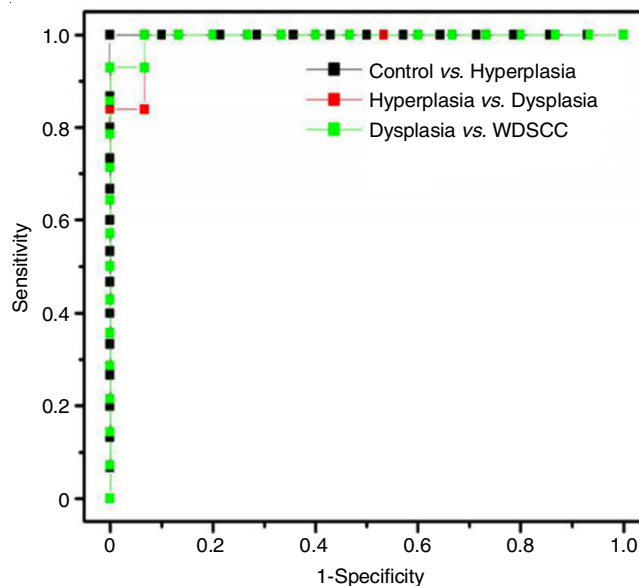
mental groups generated by PC-LDA are given in Fig. 8 and Table-4. Specificity (Sp), sensitivity (Se) and accuracy (Acc) were chosen to test the efficiency of the algorithmic model developed by PC-LDA. Receiver operating characteristic (ROC) testing is also conducted to further evaluate the performance of PC-LDA algorithms on FT-IR spectroscopy for diagnosis. The area under the curve represents an overall measure of performance; an AUC = 1 indicating a model that can perfectly discriminate between the pairwise groups, while an AUC of 0.5 is no better than random. The PC-LDA model has areas

Fig. 9. Receiver operator characteristic (ROC) curves showing the control *vs.* hyperplasia (AUC = 1.00), hyperplasia *vs.* dysplasia (AUC = 0.92) and dysplasia *vs.* WDSCC (AUC= 0.96) tissues

It is well known that pathological conditions induce significant alterations in macromolecular content, concentration, structure and dynamics in tissues and membranes. The identification and quantification of these specific molecular changes within tissues can provide diagnostic information for aiding in early detection of diseases and their optimized treatment. These changes can be determined rapidly and sensitively without using external agents by Fourier transform infrared (FT-IR) spectroscopy, since this technique monitors the vibrational modes of functional groups belonging to tissue components, such as lipids, proteins and nucleic acids [18,19]. Particularly, the whole mid region displayed an interesting pattern in which spectral differences could be associated with the tumor progression. During the tumor progression of oral musosa, lipids, proteins and other biomolecules generate significant changes in their molecular structures. Therefore, in the present study, FT-IR spectroscopic technique has been applied as a diagnostic method for monitoring the functional, structural and biochemical changes in control, hyperplasia, dysplasia and WDSCC tissues. The results of the present study demonstrated that there were pronounced spectral differences in infrared spectra between the control and experimental groups and these results revealing specific biochemical information contained in all IR-active molecules in the oral tissue samples.

In the present study, the small hump centered at ~ 3302 cm^{-1} has been appeared only in dysplasia and WDSCC tissue groups which may be associated with an increase in the relative amounts of proteins. This band is considered as a good criterion for the distinction among normal and tumorigenic conditions [20].

Lipid metabolism is an emerging field in cancer research and there is increasing evidence that lipid biomarkers should be considered a crucial hallmark of cancer [21,22]. The transformation of normal tissue into a cancerous lesion through neoplasia, hyperplasia and dysplasia is connected with qualitative and quantitative changes of lipids. Any change in lipid structure may account for pathological changes in cellular properties like variability in size/shape and alteration in the extracellular matrix observed in tumorigenic conditions. Lipid concentration and composition may thus be used as spectroscopic markers to discriminate between normal and tumor tissues. In the present study, a decrease in total lipid content of WDSCC tissues has been noticed as can be observed by an decrease in the areas of saturated lipid bands located at 2925 and 2854 cm^{-1} (Table-2). Moreover, the lipids band at 1743 cm^{-1} has been almost disappeared in WDSCC tumor tissues which may be associated with a decrease in the relative amounts of phospholipids. The decrease in the lipid concentration can be attributed to dysfunction of the cell membrane in malignancy, leading to an increase in lipids degradation. The lipid reduction in tumor tissues could be also related to the fast growth of tumor cells which need more energy [23,24]. Phospholipids are the major substrates for lipid peroxidation in cells and these changes may partly be responsible for the decrease in lipid peroxidation in tumor tissues. These results are in corroboration with previous findings [22,24].

Further, the changes in protein content and structure can be monitored by analyzing the amide I and amide II bands, which are observed at 1656 cm^{-1} and 1538 cm^{-1} respectively. As seen from Fig. 1 and Table-2, there is an significant increase in intensities as well as the areas of these bands in WDSCC and dysplasia tissues, which confirms an increase in the protein content. Since the frequency of the amide I band is sensitive to proteins conformation, this band is very useful for the determination of protein secondary structure [25]. As seen from Fig. 5, the percentage of areas obtained after curve-fitting analysis shows that the amount of β-sheet and β-turn structures were increased in the WDSCC group. Further, the amount of α-helix secondary structure decreased. These changes in the secondary structure can originate from structural rearrangements of already existing proteins or may be a result of the expression of new types of proteins with altered structure during the tumor progression. The development of tumor was characterized by a significant increase in the total protein content and the expression of new types of proteins required for cell proliferation and other cellular processes during tumor transformation. On the other hand, the total protein contents was not increased as much in hyperplasia and dysplasia tissue groups, which is supported by a significant decrease in the integrated area and the peak intensity of amide I and amide II bands. This reduction in the level of protein components indicates the controlled cell proliferation and differentiation.

As seen from Table-2, the significant increase in area values of the bands located at 1232 cm^{-1}, which originates from PO$_2$-asymmetric stretching band of nucleic acids, indicates an increase in the amount of nucleic acids in WDSCC tissue groups compared to other premalignant tissue groups. The vibrations assignable to phosphodiester groups (PO$_2$-asymmetric stretching modes) of nucleic acids are considered useful spectral biomarkers to distinguish normal from cancerous states. Thus, it is clear that DNA becomes the dominant component in tumor tissues, because tumor progression have higher proliferation rates than their normal counterparts. By considering the difference in FT-IR spectral signatures between the control and the experimental tissues, PC-LDA was carried out to distinguish the control from that of various oral transformations conditions such as hyperplasia, dysplasia and WDSCC tissues. From the statistical analysis by pair wise discriminant analysis (Fig. 8), it can clearly discriminate the control vs. hyperplasia, hyperplasia vs. dysplasia and dysplasia vs. WDSCC tissue groups. The sensitivity, specificity and accuracy of this method for control vs. hyperplasia, hyperplasia vs. dysplasia and dysplasia vs. WDSCC tissues are calculated to be sensitivity of 100, 80.95 and 85.71 %, specificities of 100, 81.18 and 90.0 % and accuracy of 100.0, 81.39 and 87.80 %, respectively. To evaluate the performance of the PC-LDA together with the LOOCV method, the ROC curve (Fig. 9) was also generated. The areas under the ROC curve for the control vs. hyperplasia, hyperplasia vs. dysplasia and dysplasia vs. WDSCC tissues were 1.00, 0.92 and 0.96, confirming that the FT-IR spectra conjunction with PC-LDA statistical method was powerful tool for discrimination of the control and the early tumor tissues.

Conclusion

The present study has shown that a FT-IR spectroscopy can be used to monitor the structural and biochemical changes

at the molecular level in various tissue transformation conditions (hyperplasia, dysplasia and WDSCC) with respect to control tissues during DMBA-induced HBP. The results revealed that a significant increase in the amount of proteins and nucleic acid contents and a decrease in the amount of lipids contents are observed in WDSCC when compared to control, hyperplasia and dysplasia. Further, the composition and secondary structure of proteins were found to be altered, which indicates some important structural alterations in the existing proteins and/or the expression of new types of proteins occurring under the tumor transformation. The present study further shows a great potential of FT-IR spectroscopy as a complimentary tool, which may provide a rapid screening method and have potential use in the diagnosis of dysplasia and early, non-invasive oral cancer.

CONFLICT OF INTEREST

The authors declare that there is no conflict of interests regarding the publication of this article.

REFERENCES

1. K. Sargeran, H. Murtomaa, S.M. Safavi, M.M. Vehkalahti and O. Teronen, *Br. J. Oral Maxillofac. Surg.*, **46**, 187 (2008); https://doi.org/10.1016/j.bjoms.2007.11.004.

2. C. Conti, P. Ferraris, E. Giorgini, T. Pieramici, L. Possati, R. Rocchetti, C. Rubini, S. Sabbatini, G. Tosi, M.A. Mariggiò and L. Lo Muzio, *J. Mol. Struct.*, **834-836**, 86 (2007); https://doi.org/10.1016/j.molstruc.2006.10.060.

3. G. Cakmak, F. Zorlu, M. Severcan and F. Severcan, *Anal. Chem.*, **83**, 2438 (2011); https://doi.org/10.1021/ac102043p.

4. N. Krishnakumar, N.K. Sulfikkarali, S. Manoharan and P. Venkatachalam, *Spectrochim. Acta A Mol. Biomol. Spectrosc.*, **115**, 648 (2013); https://doi.org/10.1016/j.saa.2013.05.076.

5. S. Turker, G. Ilbay, M. Severcan and F. Severcan, *Anal. Chem.*, **86**, 1395 (2014); https://doi.org/10.1021/ac402992j.

6. R. Zendehdel, M.N. Ali and F.H. Shirazi, *Iran. J. Pharm. Res.*, **11**, 401 (2012).

7. C. Aksoy, K.A. Kaya, B.B. Kuskonmaz, D. Uçkan and F. Severcan, *Age*, **36**, 9691 (2014); https://doi.org/10.1007/s11357-014-9691-7.

8. R. Mehrotra, G. Tyagi, D.K. Jangir, R. Dawar and N. Gupta, *J. Ovarian Res.*, **3**, 27 (2010); https://doi.org/10.1186/1757-2215-3-27.

9. G. Tosi, C. Conti, E. Giorgini, P. Ferraris, M.G. Garavaglia, S. Sabbatini, S. Staibano and C. Rubini, *Analyst*, **135**, 3213 (2010); https://doi.org/10.1039/c0an00505c.

10. A.D. Surowka, D. Adamek and M. Szczerbowska-Boruchowska, *Analyst*, **140**, 2428 (2015); https://doi.org/10.1039/C4AN01867B.

11. J. Anastassopoulou, E. Boukaki, C. Conti, P. Ferraris, E. Giorgini, C. Rubini, S. Sabbatini, T. Theophanides and G. Tosi, *Vib. Spectrosc.*, **51**, 270 (2009); https://doi.org/10.1016/j.vibspec.2009.07.005.

12. P.D. Lewis, K.E. Lewis, R. Ghosal, S. Bayliss, A.J. Lloyd, J. Wills, R. Godfrey, P. Kloer and L.A. Mur, *BMC Cancer*, **10**, 640 (2010); https://doi.org/10.1186/1471-2407-10-640.

13. S. Sabbatini, C. Conti, C. Rubini, V. Librando, G. Tosi and E. Giorgini, *Vib. Spectrosc.*, **68**, 196 (2013); https://doi.org/10.1016/j.vibspec.2013.07.002.

14. M. Gohulkumar, S.S. Nazeer, R.S. Jayasree, K. Gurushankar and N. Krishnakumar, *Anal. Methods*, **6**, 9744 (2014); https://doi.org/10.1039/C4AY01877J.

15. K. Gurushankar, S.S. Nazeer, M. Gohulkumar, R.S. Jayasree and N. Krishnakumar, *RSC Adv.*, **4**, 46896 (2014); https://doi.org/10.1039/C4RA06140C.

16. P.L.R.M. Palaniappan and K.S. Pramod, *Food Chem. Toxicol.*, **48**, 2337 (2010); https://doi.org/10.1016/j.fct.2010.05.068.

17. S. Garip and F. Severcan, *J. Pharm. Biomed. Anal.*, **52**, 580 (2010); https://doi.org/10.1016/j.jpba.2010.01.044.

18. G.E. Menzies, H.R. Fox, C. Marnane, L. Pope, V. Prabhu, S. Winter, A.V. Derrick and P.D. Lewis, *Transl. Res.*, **163**, 19 (2014); https://doi.org/10.1016/j.trsl.2013.09.006.

19. S. Kalmodia, S. Parameswaran, W. Yang, S. Krishnakumar and C.J. Barrow, *Sci. Rep.*, **5**, 16649 (2015); https://doi.org/10.1038/srep16649.

20. R. Eckel, H. Huo, H.W. Guan, X. Hu, X. Che and W.D. Huang, *Vib. Spectrosc.*, **27**, 165 (2001); https://doi.org/10.1016/S0924-2031(01)00134-5.

21. T. Meyer, O. Guntinas-Lichius, F. Von Eggeling, G. Ernst, D. Akimov, M. Schmitt, B. Dietzek and J. Popp, *Head Neck*, **9**, E35 (2013); https://doi.org/10.1002/hed.23139.

22. H. Abramczyk, J. Surmacki, M. Kopec, A.K. Olejnik, K. Lubecka-Pietruszewska and K. Fabianowska-Majewska, *Analyst*, **140**, 2224 (2015); https://doi.org/10.1039/C4AN01875C.

23. H. Abramczyk, B. Brozek-Pluska, J. Surmacki, J. Jablonska-Gajewicz and R. Kordek, *Prog. Biophys. Mol. Biol.*, **108**, 74 (2012); https://doi.org/10.1016/j.pbiomolbio.2011.10.004.

24. R. Munir, H. Usman, S. Hasnain, K. Smans, H. Kalbacher and N. Zaidi, *Biochimie*, **102**, 9 (2014); https://doi.org/10.1016/j.biochi.2014.03.010.

25. O. Bozkurt, M. Severcan and F. Severcan, *Analyst*, **135**, 3110 (2010); https://doi.org/10.1039/c0an00542h.